Hamburger Beiträge
zur Angewandten Mathematik

An application of the finite volume method to the thermoregulation of infants

Bernd Fischer, Martin Ludwig and Andreas Meister

Reihe F
Computational Fluid Dynamics and Data Analysis 12
February 2000

Hamburger Beiträge zur Angewandten Mathematik

Reihe A	Preprints
Reihe B	Berichte
Reihe C	Mathematische Modelle und Simulation
Reihe D	Elektrische Netzwerke und Bauelemente
Reihe E	Scientific Computing
Reihe F	Computational Fluid Dynamics and Data Analysis

An application of the finite volume method to the thermoregulation of infants

Bernd Fischer [1], Martin Ludwig and Andreas Meister [2]

Abstract A mathematical model is developed and used for a computer simulation of the thermoregulation of premature infants. We propose a finite volume technique for the solution of the associated partial differential equation on an unstructured grid. Emphasis is laid on the model and the validation of the numerical scheme. Beside various test runs using real life data, we present a discrete maximum principle for the steady state solution with respect to the non-convex computational domain.

Keywords: Finite volume method, Thermoregulation, Maximum principle.

1 Introduction

Severe asphyxia of the fetus or newborn is known to be an important cause of injury to the developing brain (Mallard et al., 1995). Experimental studies have shown (Gluckman and Williams, 1992) that the neuronal loss evolves over several days. There are various factors that may influence the degree and regional distribution of neuronal loss, one of which is the cerebral temperature. Studies in both adult and immature animals have shown that lowering the cerebral temperature after a hypoxic-ischaemic insult can markedly protect the brain from damage (see, e.g., Busto et al., 1989)

It is an open question, whether it is possible to lower the cerebral temperature of an infant by 2-3°C and still to maintain a comfortable temperature for the rest of the body by changing the environmental parameters in the incubator. The specific objective of this investigation is the development of a mathematical model and computer simulation for the analysis of this and related questions.

In Section 2 we outline the derivation of a two dimensional model of human thermoregulation. Sick or premature infants are generally smaller and sometimes less developed than their healthy full-term counterparts. This results in a differentiation of thermal care required for different size neonates in order to achieve the desired degree of thermoregulation. Therefore, we propose a model which is easily adapted to the required sizes of the body. The price paid for this freedom is the need to deal with unstructured grids. This is done by employing a finite volume technique. We comment on this approach in Section 3. For using the proposed simulation within a clinical environment a sound validation of the model as well as of the numerical scheme is necessary. To this end, we prove in Section 3 a discrete maximum principle

[1] Institute of Mathematics, Medical University of Lübeck, Germany

[2] Institut für Angewandte Mathematik, Universität Hamburg, Bundesstraße 55, D-20146 Hamburg, Germany

for the steady state solution even though the computational domain is non-convex. Finally, in Section 4 we present a variety of numerical test runs with respect to real life data.

2 Governing equation

In this section we briefly introduce a mathematical model of human thermoregulation. We follow the derivation of Werner and Webb (1993). However, in their approach they considered a two dimensional six-cylinder model assuming purely radial heat conduction within the cylindrical elements. In contrast, we use a more realistic two dimensional geometry $D \subset \mathbb{R}^2$ (compare figure 1) for the infant without any restriction concerning the heat conduction. To our best knowledge, this is the first time that such a complex geometry and model has been considered for the simulation of the heat transfer in a human body. For a review on developments in this direction up to the nineties we refer to Werner (1989).
It is well known that the so-called *heat equation*

$$\begin{aligned} c(\mathbf{x})\rho(\mathbf{x})\partial_t T(\mathbf{x},t) &= \operatorname{div}\left(\lambda(\mathbf{x})\nabla T(\mathbf{x},t)\right) \\ &= \partial_{x_1}(\lambda\partial_{x_1}T)(\mathbf{x},t) + \partial_{x_2}(\lambda\partial_{x_2}T)(\mathbf{x},t),\ \mathbf{x}\in D,\ t\in\mathbb{R}^+, \end{aligned} \tag{2.1}$$

in the absence of any heat sources or sinks, describes the temperature distribution $T(\mathbf{x},t)$ in the domain D for the time $t > 0$. Here, $\lambda(\mathbf{x})$ denotes the heat conductivity of the tissue, $c(\mathbf{x})$ its specific heat and $\rho(\mathbf{x})$ its density, respectively.
For living tissue the passage of blood modifies the heat transfer process. Furthermore, metabolic processes generate heat within the tissue. A formulation, sometimes called the *bio-heat equation*, taking these factors into account looks like

$$c(\mathbf{x})\rho(\mathbf{x})\partial_t T(\mathbf{x},t) = \operatorname{div}\left(\lambda(\mathbf{x})\nabla T(\mathbf{x},t)\right) + f(\mathbf{x},t), \tag{2.2}$$

where

$$f(\mathbf{x},t) = Q_M(\mathbf{x},t) + Q_B(\mathbf{x},t). \tag{2.3}$$

Here, $Q_M(\mathbf{x},t) = Q_M(\mathbf{x})$ is the rate of metabolic heat production. Furthermore, Q_B should model the heat transfer within the body due to the bloodstream. More precisely, we set

$$Q_B(\mathbf{x},t) = c_B(\mathbf{x})\rho_B(\mathbf{x})K_B(\mathbf{x})BF(\mathbf{x})(T_B(t) - T(\mathbf{x},t)), \tag{2.4}$$

where $c_B(\mathbf{x})$ and $\rho_B(\mathbf{x})$ denote the specific heat and density of blood, respectively. Moreover, $BF(\mathbf{x})$ represents the blood-flow whereas $K_B(\mathbf{x})$ is a so-called counter current factor taking into account the fact that the temperatures of arterial and venous blood interact with each other. Finally, $T_B(t)$ denotes the temperature of the blood. For simplicity, we assume that it does not depend on $\mathbf{x}$ and is determined by the following average

$$T_B(t) = \frac{\int_D K_B(\mathbf{x})BF(\mathbf{x})T(\mathbf{x},t)d\mathbf{x}}{\int_D K_B(\mathbf{x})BF(\mathbf{x})d\mathbf{x}}. \tag{2.5}$$

In summary, Q_B represents the difference between the heat flow input and the heat flow output through blood.
It is worthwhile to note that the model assumption (2.5) is satisfied at least for the steady state case $\partial_t T(\mathbf{x}, t) = 0$. Actually, we are only interested in the solution of the steady state equation

$$\operatorname{div}(\lambda(\mathbf{x})\nabla T(\mathbf{x}, t)) + f(\mathbf{x}, t) = 0. \tag{2.6}$$

To solve this equation we apply a time-marching procedure to the time-dependent equation (2.2) with the simple setting $c(\mathbf{x}) = \rho(\mathbf{x}) = 1$.
Finally, we supplement the bio-heat equation (2.2) by the initial condition

$$T(\mathbf{x}, 0) = T_0(\mathbf{x}),\ \mathbf{x} \in D,$$

and the Dirichlet boundary condition

$$T(\mathbf{x}, t) = T_{\partial D}(\mathbf{x}, t),\ \mathbf{x} \in \partial D,\ t \in \mathbb{R}_0^+.$$

The latter condition enables one to assign temperature to the body surface and therefore to model the environmental settings like air temperature in the incubator and temperature of the mattress. Also, the cooling of the head might be imposed by appropriate Dirichlet data.

2.1 Analysis of the governing equation

This section contains two theorems which are direct conclusions from the maximum principle of E. Hopf (see, e.g., Protter and Weinberger, 1967). They refer to our governing equation (2.6) if its source terms are neglected and some additional assumptions are made. Theorem 2.1 states that the occurrence of a temperature maximum in the interior of the computational domain D implies a constant temperature distribution in $\overline{D}$. Theorem 2.2 constitutes the remarkable result that the temperature distribution attains its maximum and minimum on the boundary ∂D. Therefore the equilibrium temperature always lies between the maximum and minimum values of the prescribed boundary temperature.

Theorem 2.1 *Let $D \subset \mathbb{R}^n$ be a bounded domain,*

$$\mathbf{A} = (a_{ij})_{i,j=1,\ldots,n} : D \to M(n \times n, \mathbb{R})$$

a map which satisfies $\mathbf{A}(\mathbf{x}) = (\mathbf{A}(\mathbf{x}))^T \quad \forall \mathbf{x} \in D$ and $\mathbf{b} = (b_i)_{i=1,\ldots,n} : D \to \mathbb{R}^n$. Suppose the functions a_{ij}, b_i are bounded in D and the operator

$$L : C^2(D, \mathbb{R}) \to ABB(D, \mathbb{R})$$
$$L[u] := \textstyle\sum_{i,j=1}^n a_{ij} \dfrac{\partial^2 u}{\partial x_i \partial x_j} + \sum_{i=1}^n b_i \dfrac{\partial u}{\partial x_i}$$

is uniformly elliptic in D ($ABB(D,\mathbb{R})$ denotes the real space of all real-valued functions defined in D). Let $T \in C(\overline{D},\mathbb{R})$ be a function which is twice continously differentiable in D and which satisfies the inequality

$$L[T|_D](\mathbf{x}) \geq 0 \ \forall \mathbf{x} \in D.$$

If there is a point $\mathbf{y} \in D$ with $T(\mathbf{x}) \leq T(\mathbf{y}) \ \forall \mathbf{x} \in D$ then T is constant, i.e. $T(\mathbf{x}) = T(\mathbf{y}) \ \forall \mathbf{x} \in \overline{D}$.

Theorem 2.2 *Let $D \subset \mathbb{R}^n$ be a bounded domain,*

$$\mathbf{A} = (a_{ij})_{i,j=1,\ldots,n} : D \to M(n \times n, \mathbb{R})$$

a map which satisfies $\mathbf{A}(\mathbf{x}) = (\mathbf{A}(\mathbf{x}))^T \quad \forall \mathbf{x} \in D$ and $\mathbf{b} = (b_i)_{i=1,\ldots,n} : D \to \mathbb{R}^n$. Suppose the functions a_{ij}, b_i are bounded in D and the operator

$$L : C^2(D,\mathbb{R}) \to ABB(D,\mathbb{R})$$
$$L[u] := \textstyle\sum_{i,j=1}^n a_{ij} \dfrac{\partial^2 u}{\partial x_i \partial x_j} + \textstyle\sum_{i=1}^n b_i \dfrac{\partial u}{\partial x_i}$$

is uniformly elliptic in D. Let $T \in C(\overline{D},\mathbb{R})$ be a function which is twice continously differentiable in D and which satisfies the inequality

$$L[T|_D](\mathbf{x}) \geq 0 \ \forall \mathbf{x} \in D.$$

Then T attains its maximum and minimum at the boundary of the domain, i.e. there exist $\mathbf{x}', \mathbf{x}'' \in \partial D$ such that

$$T(\mathbf{x}) \leq T(\mathbf{x}') \ \forall \mathbf{x} \in \overline{D} \quad \textit{and} \quad T(\mathbf{x}'') \leq T(\mathbf{x}) \ \forall \mathbf{x} \in \overline{D}.$$

3 Finite volume approximation

Time-dependent partial differential equations (e.g. Euler and Navier-Stokes equations) are often solved numerically although one is only interested in steady state solutions. The advantage of this procedure is based on the fact that it opens a wide field of well-known, highly efficient and reliable numerical methods, which can be employed to compute both steady as well as unsteady solutions in the same manner. Thus, we intend to develop a numerical method for the time-dependent heat equation

$$\partial_t T(\mathbf{x},t) = \operatorname{div}\left(\lambda(\mathbf{x}) \nabla T(\mathbf{x},t)\right) + f(\mathbf{x},t), \ \mathbf{x} \in D, \ t \in \mathbb{R}^+, \tag{3.1}$$

where the source term f is given by

$$f(\mathbf{x},t) = Q_M(\mathbf{x}) + Q_B(\mathbf{x},t), \ \mathbf{x} \in D, \ t \in \mathbb{R}_0^+.$$

Additionally, we require (3.1) to hold on the bounded domain $D \subset \mathbb{R}^2$ under the initial conditions

$$T(\mathbf{x},0) = T_0(\mathbf{x}), \ \mathbf{x} \in D,$$

as well as boundary conditions

$$T(\mathbf{x},t) = T_{\partial D}(\mathbf{x},t),\ \mathbf{x} \in \partial D,\ t \in \mathbb{R}_0^+.$$

Setting $T_{\partial D}(\mathbf{x},t) = T_{\partial D}(\mathbf{x})$, $t \in \mathbb{R}_0^+$, it is obvious that a temperature distribution satisfying the initial boundary value problem as well as $\partial_t T(\mathbf{x},t) = 0$ represents a solution of the boundary value problem (2.6), which obviously is also a steady state solution of equation (2.2).

In finite volume approximations the needs concerning the treatment of complicated geometries and adaptation as well as the needs for robust and accurate algorithms are perfectly matched. Finite volume methods are formulated on general control volumes and well-known successful time stepping schemes and spatial discretization techniques can easily be employed in the general framework (see, e.g., Sonar, 1993; Meister, 1998). Therefore, we consider the integral form of the equation (3.1), namely

$$\frac{d}{dt}\int_\sigma T(\mathbf{x},t)\,d\mathbf{x} = \int_{\partial\sigma} \lambda(\mathbf{x})\nabla T^T(\mathbf{x},t)\mathbf{n}(\mathbf{x})\,ds + \int_\sigma f(\mathbf{x},t)\,d\mathbf{x} \tag{3.2}$$

for all control volumes $\sigma \subset D$.

In order to solve equation (3.2) numerically by means of a finite volume method, the space part $\overline{D}$ has to be decomposed into a finite number of sub-domains. For simplicity, we assume the boundary $\partial D = \overline{D} \setminus D$ to be smooth in the sense that it can be approximated by a finite number of straight lines in a sufficient accurate manner (for example, ∂D is piecewise polygonal).

We start from an arbitrary conforming triangulation $\mathcal{D}^h$ of the domain $\overline{D}$ which is called the primary mesh consisting of finitely many (say $\#\mathcal{D}^h$) triangles $\mathcal{D}_i$, $i = 1,\ldots,\#\mathcal{D}^h$. Thereby, the parameter h corresponds to a typical one-dimensional geometrical measure of the triangulation, as, for example, the maximum diameter of the smallest inclosing circle of the triangle $\mathcal{D}_i$, $i = 1,\ldots,\#\mathcal{D}^h$. For a comprehensive definition of a primary grid we refer to Sonar (1997). Furthermore, $\mathcal{N}^h$ denotes the index set of all nodes of the triangulation $\mathcal{D}^h$ and is subdivided by $\mathcal{N}^h = \mathcal{N}^{h,D} \cup \mathcal{N}^{h,\partial D}$, where $\mathcal{N}^{h,D}$ is associated with the inner points and $\mathcal{N}^{h,\partial D}$ includes the indices of the boundary points. We set $N := \#\mathcal{N}^h$ and denote the three edges of the triangle $\mathcal{D}$ by $e_{\mathcal{D},k}$, $k = 1,2,3$. Furthermore, we define

$$E(i) = \left\{e_{\mathcal{D},k} \mid k \in \{1,2,3\}, \mathcal{D} \in \mathcal{D}^h,\ \text{node } \mathbf{x}_i \in e_{\mathcal{D},k}\right\},$$

$$V(i) = \left\{\mathcal{D} \mid \text{node } \mathbf{x}_i \text{ is vertex of } \mathcal{D} \in \mathcal{D}^h\right\},$$

and

$$C(\mathcal{D}) = \{i \mid i \in \{1,\ldots,N\},\ \text{node } \mathbf{x}_i \text{ is vertex of } \mathcal{D}\}.$$

In order to achieve an appropriate resolution of the skin, fat, and bone areas, we define inner points within this three tissues in a structured manner. Inside the kernel we make use of an algorithm developed by Friedrich (1993) for the generation of inner points in two dimensional triangulations which provides mostly isotropic triangles. Starting from all points $\mathbf{x}_i$, $i \in \mathcal{N}^h$, the method described in Friedrich (1993) is employed to generate the final conforming triangulation (see figures 1 and 2).

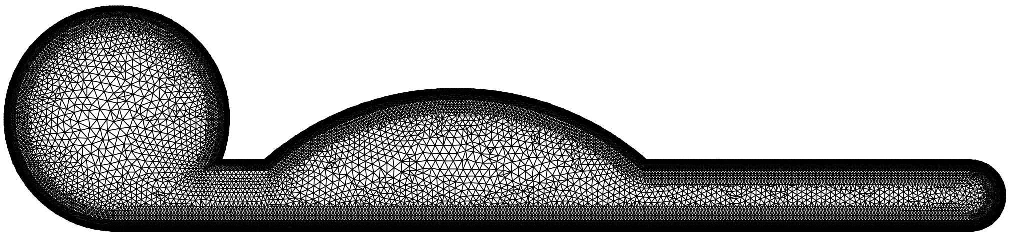

Figure 1: Primary mesh

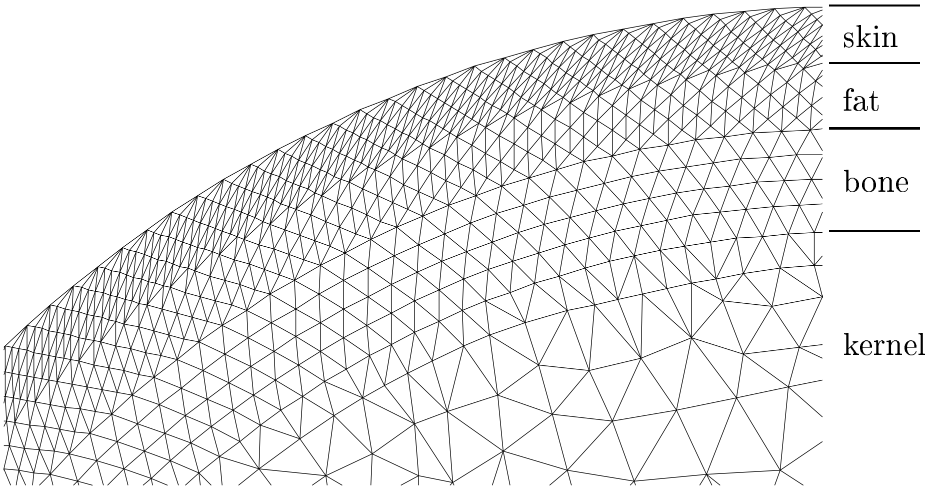

Figure 2: Primary mesh and tissue layers in the head region

As we see in the following, the occurrence of second order derivatives within the partial differential equation requires the evaluation of first order derivative on the boundary of each control volume used in the finite volume scheme. Due to this fact we decided to employ a box type method where the computation of a first order derivative on the boundary of each box is straightforward.
We define a discrete control volume σ_i as the open subset of $\mathbb{R}^2$ including the node $\mathbf{x}_i = (x_{i1}, x_{i2})^T$ and bounded by the straight lines, which are defined by the connection of the midpoint of the edge $e_{\mathcal{D},k} \in E(i)$ with the barycentre $\mathbf{x}_s = (x_{s1}, x_{s2})^T = \frac{1}{3}\sum_{i \in C(\mathcal{D})} \mathbf{x}_i$ of the corresponding triangle $\mathcal{D}$ (see figure 3). In the case that $\mathbf{x}_i$ is on the boundary of the computational domain, the line defined by the connection of the midpoint of the boundary edge and the node itself is also a part of $\partial\sigma_i$. The union $\mathcal{B}^h$ of all boxes σ_i, $i \in \mathcal{N}^h$, is called the secondary mesh. Let $N(i)$ denote the index set of all nodes neighboring node $\mathbf{x}_i$, i.e. those nodes $\mathbf{x}_j$, $j \neq i$, for which $\int\limits_{\partial\sigma_i \cap \partial\sigma_j} 1 \; ds \neq 0$ is valid. In general, for $j \in N(i)$ the boundary between the control volume σ_i and σ_j consists of two line segments which are denoted by l_{ij}^k, $k = 1, 2$. Furthermore, $\mathbf{n}_{ij}^k$, $k = 1, 2$, represent the accompanying unit normal

vectors.
A finite volume method represents a discretization of the evolutionary equation (3.2) for cell averages which are defined by means of the cell average operator

$$\left(\mathcal{M}_h T\right)(t)|_\sigma := \frac{1}{|\sigma|}\int_\sigma T(\mathbf{x},t)\; d\mathbf{x},$$

where $|\sigma|$ denotes the volume of the box σ. With regard to the secondary mesh $\mathcal{B}^h$ we can rewrite the integral form of the heat equation as

$$\frac{d}{dt}\left(\mathcal{M}_h T\right)(t)|_{\sigma_i} = \left(\mathcal{L}_\nu^h T\right)(t)|_{\sigma_i} + \left(\mathcal{L}_s^h T\right)(t)|_{\sigma_i}, \;\; \forall \sigma_i \in \mathcal{B}^h, \tag{3.3}$$

where the operators $\mathcal{L}_\nu^h$ and $\mathcal{L}_s^h$ are defined to be

$$\left(\mathcal{L}_\nu^h T\right)(t)|_{\sigma_i} = \frac{1}{|\sigma_i|}\int_{\partial\sigma_i} \lambda(\mathbf{x})\nabla T^T(\mathbf{x},t)\mathbf{n}(\mathbf{x})\; ds$$

and

$$\left(\mathcal{L}_s^h T\right)(t)|_{\sigma_i} = \frac{1}{|\sigma_i|}\int_{\sigma_i} f(\mathbf{x},t)\; d\mathbf{x}.$$

Furthermore $T_i(t) := \left(\mathcal{M}_h T\right)(t)|_{\sigma_i}$ and the initialization of the piecewise constant temperature is computed by the cell average operator applied to the given initial temperature distribution $T_i(0) := \left(\mathcal{M}_h T\right)(0)|_{\sigma_i}$, $\forall \sigma_i \in \mathcal{B}^h$. The discrete boundary temperature distribution is considered as piecewise constant along each boundary part $\partial\sigma_i \cap \partial D$, $i \in \mathcal{N}^{h,\partial D}$, which should correspond to the definition of the cell averages and is determined by

$$T_{i,\partial D}(\mathbf{x}) = \frac{1}{|\partial\sigma_i \cap \partial D|}\int\limits_{\partial\sigma_i\cap\partial D} T_{\partial D}(\mathbf{y})\; ds,\; \mathbf{x} \in \partial\sigma_i \cap \partial D,\; i \in \mathcal{N}^{h,\partial D}. \tag{3.4}$$

3.1 Discretization of the boundary integral

Taking account of the secondary mesh $\mathcal{B}^h$, the boundary integral operator can be expressed as

$$\begin{aligned}\left(\mathcal{L}_\nu^h T\right)(t)|_{\sigma_i} &= \frac{1}{|\sigma_i|}\Bigg\{\sum_{j\in N(i)}\sum_{k=1}^{2}\int_{l_{ij}^k} \lambda(\mathbf{x})\nabla T^T(\mathbf{x},t)\mathbf{n}_{ij}^k\; ds \\ &\qquad + \int_{\partial\sigma_i\cap\partial D} \lambda(\mathbf{x})\nabla T^T(\mathbf{x},t)\mathbf{n}(\mathbf{x})\; ds\Bigg\}.\end{aligned} \tag{3.5}$$

Let $\mathcal{D}_{ij}$ denote the triangle which contains the line segment l_{ij}^k. For the evaluation of the flux over the edge l_{ij}^k we approximate the heat coefficient by means of the arithmetic mean value $\lambda_{\mathcal{D}_{ij}} = \frac{1}{3}\sum_{m\in C(\mathcal{D}_{ij})}\lambda(\mathbf{x}_m)$. Furthermore, the gradient of the temperature is calculated using the unique linear distribution of T on the triangle $\mathcal{D}_{ij}$ in the form

$$\nabla T_{\mathcal{D}_{ij}}(t) = \frac{1}{det}\begin{pmatrix} x_{m2}-x_{i2} & x_{i2}-x_{j2} \\ x_{i1}-x_{m1} & x_{j1}-x_{i1} \end{pmatrix} \cdot \begin{pmatrix} T_j(t)-T_i(t) \\ T_m(t)-T_i(t) \end{pmatrix},$$

where $det = (x_{j1}-x_{i1})(x_{m2}-x_{i2}) - (x_{m1}-x_{i1})(x_{j2}-x_{i2})$ and $i,j,m \in C(\mathcal{D}_{ij})$. The combination of the described procedure leads directly to the formulation of a numerical flux function

$$H_\nu\left(T_i(t), T_j(t), T_m(t); \mathbf{n}_{ij}^k\right) = \lambda_{\mathcal{D}_{ij}} \nabla T_{\mathcal{D}_{ij}}^T(t)\ \mathbf{n}_{ij}^k \tag{3.6}$$

and consequently, for each inner control volume (i.e. $i \in \mathcal{N}^{h,D}$) we obtain

$$\left(\mathcal{L}_\nu^h T\right)(t)|_{\sigma_i} = \frac{1}{|\sigma_i|}\sum_{j\in N(i)}\sum_{k=1}^{2} H_\nu\left(T_i(t), T_j(t), T_m(t); \mathbf{n}_{ij}^k\right)|l_{ij}^k|.$$

In the case of Neumann boundary conditions the evaluation of the boundary integral

$$\int_{\partial\sigma_i\cap\partial D} \lambda(\mathbf{x})\nabla T^T(\mathbf{x},t)\mathbf{n}(\mathbf{x})\ ds \tag{3.7}$$

is directly determined by the boundary conditions and hence no expensive numerical approximation is necessary. Dirichlet boundary conditions as considered here are much more complicated. An appropriate numerical approximation of the remaining second boundary integral in equation (3.5) is required in order to ensure a discrete maximum principle in our numerical framework. Utilizing the notation introduced within figure 3 we define

$$\mathbf{c}_i = \mathbf{x}_i - \frac{\sqrt{3}\rho_i}{4\|\mathbf{n}_{ij}+\mathbf{n}_{im}\|_2}(\mathbf{n}_{ij}+\mathbf{n}_{im}), \tag{3.8}$$

where $\mathbf{n}_{i\ell}$, $\ell = j,m$, represents the outer unit normal vector on $l_{i\ell}$, $\ell = j,m$, and the weight ρ_i is given by

$$\rho_i = \frac{1}{2}\min\{\|\mathbf{x}_j - \mathbf{x}_i\|_2\,|j \in N(i)\cap C(\mathcal{D})\}.$$

Obviously, the point $\mathbf{c}_i$ is always located in the interior of the box σ_i and straightforward calculations prove that $\mathbf{c}_i$ equals the barycentre of the corresponding control volume, if $V(i)$ consists exclusively of isotropic triangles and the two line segments $l_{ij}, l_{im} \in \partial\sigma_i \cap \partial D$ are parallel. Furthermore, each triangle $\mathcal{D}_{ij}^{\mathbf{c}}$ build by $\mathbf{c}_i$, $\mathbf{x}_i$ and $\mathbf{x}_{ij} = \frac{1}{2}(\mathbf{x}_i+\mathbf{x}_j)$, $j \in N(i)\cap\mathcal{N}^{h,\partial D}$, satisfies $\mathcal{D}_{ij}^{\mathbf{c}} \subset D$.
Having introduced the boundary triangle $\mathcal{D}_{i\ell}^{\mathbf{c}}$, $\ell = j,m$, as described above and constituting $T_i(t)$ to be located at the extended barycentre $\mathbf{c}_i$, the remaining boundary integral (3.7) is discretized as

$$\int_{\partial\sigma_i\cap\partial D} \lambda(\mathbf{x})\nabla T^T(\mathbf{x},t)\mathbf{n}(\mathbf{x})\ ds = \delta_i \sum_{\ell\in\{j,m\}} H_\nu(T_i(t), T_{i,\partial D}(\mathbf{x}_i), T_{i,\partial D}(\mathbf{x}_{i\ell}); \mathbf{n}_{i\ell})\,|l_{i\ell}|, \tag{3.9}$$

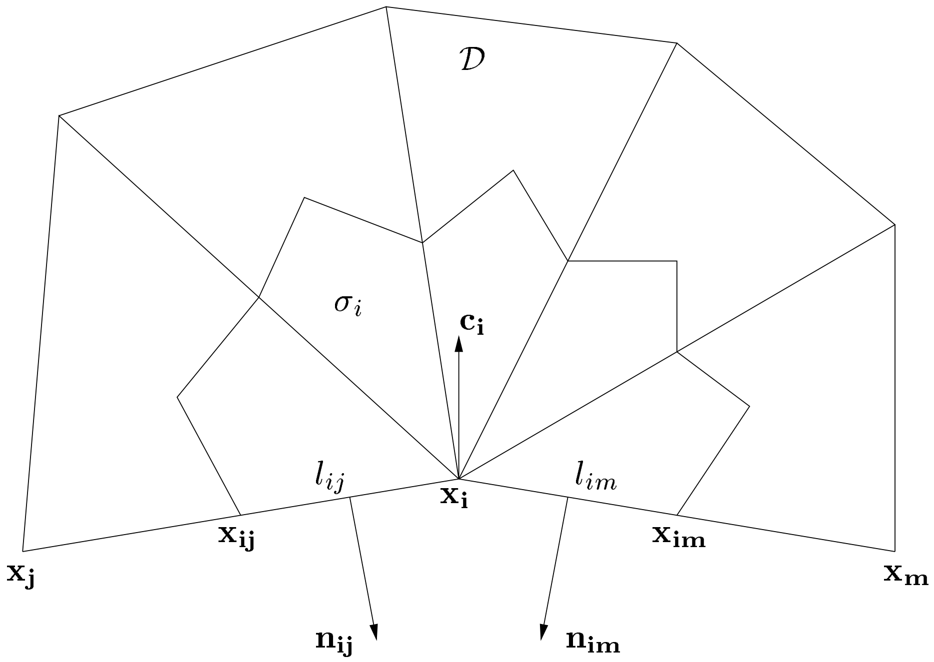

Figure 3: Boundary control volume

where

$$\delta_i = \begin{cases} 1 & \text{, if } i \in \mathcal{N}^{h,\partial D} \\ 0 & \text{, otherwise.} \end{cases}$$

3.2 Discretization of the source term

The source term including the specific metabolic heat production and the specific heat transport via small vessels (2.4) is approximately evaluated by

$$\int_{\sigma_i} Q_M(\mathbf{x})\, d\mathbf{x} = \underbrace{|\sigma_i| Q_M(\mathbf{x}_i)}_{=H_{S,i}^M},\ i \in \mathcal{N}^h$$

and

$$\int_{\sigma_i} Q_B(\mathbf{x},t)\, d\mathbf{x} = H_{S,i}^B(T_1(t),\ldots,T_N(t)),\ i \in \mathcal{N}^h,$$

where

$$H_{S,i}^B(T_1(t),\ldots,T_N(t)) = |\sigma_i| \rho_{BL} c_{BL} BF(\mathbf{x}_i) \left(\frac{\sum_{j=1}^N |\sigma_j| K(\mathbf{x}_j) BF(\mathbf{x}_j) T_j(t)}{\sum_{j=1}^N |\sigma_j| K(\mathbf{x}_j) BF(\mathbf{x}_j)} - T_i(t) \right).$$

Thus, the approximation of the source term becomes

$$\left(\mathcal{L}_s^h T\right)(t)|_{\sigma_i} = \frac{1}{|\sigma_i|} \Big\{ H_{S,i}^M + H_{S,i}^B(T_1(t),\ldots,T_N(t)) \Big\}.$$

3.3 Time discretization

As announced, we use a time-marching procedure in order to reach the steady state solution of the time-dependent heat equation (3.2). We integrate the integral form of the equation from the time level t^n to the time level $t^{n+1} = t^n + \Delta t$, using the Θ-scheme

$$
\begin{aligned}
\Delta T_i \;=\; \frac{\Delta t}{|\sigma_i|}\Bigg\{ & \sum_{j\in N(i)} \sum_{k=1}^{2} \Big\{\Theta_1 H_\nu\left(T_i(t^{n+1}), T_j(t^{n+1}), T_m(t^{n+1}); \mathbf{n}_{ij}^k\right) \\
& \qquad + (1-\Theta_1) H_\nu\left(T_i(t^n), T_j(t^n), T_m(t^n); \mathbf{n}_{ij}^k\right)\Big\}\, |l_{ij}^k| \\
& + \delta_i \sum_{\ell\in j,m} \Big\{\Theta_1 H_\nu(T_i(t^{n+1}), T_{i,\partial D}(\mathbf{x}_i), T_{i,\partial D}(\mathbf{x}_{i\ell}); \mathbf{n}_{i\ell}) \\
& \qquad + (1-\Theta_1) H_\nu(T_i(t^n), T_{i,\partial D}(\mathbf{x}_i), T_{i,\partial D}(\mathbf{x}_{i\ell}); \mathbf{n}_{i\ell})\Big\}\, |l_{i\ell}| \\
& + \Theta_2 H_{S,i}^B(T_1(t^{n+1}), \ldots, T_N(t^{n+1})) \\
& + (1-\Theta_2) H_{S,i}^B(T_1(t^n), \ldots, T_N(t^n)) + H_{S,i}^M \Bigg\},
\end{aligned}
$$

where $\Delta T_i = T_i(t^{n+1}) - T_i(t^n)$. Since we are only interested in steady state solutions it is not neccessary to employ a higher order time stepping scheme. $\Theta_1 = \Theta_2 = 0$ leads to an explicit scheme. However, independent of the occurrence of source terms, it is well-known that due to stability reasons these schemes are limited by a CFL number by 1 which is a severe upper bound for simulations of parabolic equations especially on adapted or highly stretched grids. A suitable way to overcome this restriction is an implicit discretization (e.g. $\Theta_1 = \Theta_2 = 1$), which inherently satisfies the CFL condition. Therefore, the flux function H_ν as well as the source term due to blood flow $H_{S,i}^B$ have to be evaluated at the time level t^{n+1}. Unfortunately, introducing a Taylor series expansion, the global dependence of the blood flow leads to a full matrix which is usually impractical to work with since the storage requirements cannot be satisfied, in general. It is hence usually impossible to use $\Theta_2 \neq 0$ and consequently we propose to employ $\Theta_1 = 1$ and $\Theta_2 = 0$ and thus the linear system

$$
\mathbf{A}\boldsymbol{\Delta}\mathbf{T} = \mathbf{b}, \;\; \boldsymbol{\Delta}\mathbf{T} = (\Delta T_1, \ldots, \Delta T_N)^T \tag{3.10}
$$

arising from the linearization of the flux function H_ν contains a sparse matrix $\mathbf{A}$ in the sense that $A_{ij} = 0$, $\forall j \notin N(i)$ hold for $i \in \mathcal{N}^h$. Note, that the right hand side $\mathbf{b}$ contains the explicit fluxes and source terms and that the matrix $\mathbf{A}$ reduces to the identity matrix in the case that $\Theta_1 = \Theta_2 = 0$. A brief description of the chosen iterative method for solving the linear system (3.10) will be provided within section 4.

3.4 Analysis of the finite volume scheme

Our final goal in this section is to prove that the steady state solution achieved by the developed numerical method satisfies the discrete analogue of the maximum principles given by theorem 2.1 and theorem 2.2 if the source terms are neglected. We assume that the triangulation is well chosen in the sense that for each triangle $\mathcal{D} \in \mathcal{D}^h$ the maximum angle inside $\mathcal{D}$ is less or equal $90°$.
The preliminary steps in our discrete analysis are to define some basic properties concerning the fluxes within each triangle, separately.

Lemma 3.1 *Consider an arbitrary triangle $\mathcal{D} \in \mathcal{D}^h$ and assume that the corresponding cell average $T_i(t^n)$, $i \in C(\mathcal{D})$ satisfies*

$$T_i(t^n) = \max_{j \in C(\mathcal{D})} T_j(t^n) \quad \left(T_i(t^n) = \min_{j \in C(\mathcal{D})} T_j(t^n) \right).$$

Then, the local update of the cell average $T_i(t^n)$ associated with the triangle $\mathcal{D}$

$$\Delta T_i|_{\mathcal{D}} = H_\nu \left(T_i(t^n), T_j(t^n), T_m(t^n); \mathbf{n}_{ij}\right)|l_{ij}| + H_\nu \left(T_i(t^n), T_j(t^n), T_m(t^n); \mathbf{n}_{im}\right)|l_{im}|$$

satisfies

$$\Delta T_i|_{\mathcal{D}} \leq 0 \quad (\Delta T_i|_{\mathcal{D}} \geq 0).$$

Proof: By using the orthogonal matrix

$$\mathbf{B} = \begin{pmatrix} 0 & 1 \\ -1 & 0 \end{pmatrix},$$

and the midpoints $\xi = \frac{1}{2}(\mathbf{x}_i + \mathbf{x}_j)$, $\eta = \frac{1}{2}(\mathbf{x}_i + \mathbf{x}_m)$, we can write the unit outer normal vectors in the form

$$\mathbf{n}_{ij} = \frac{1}{|l_{ij}|}\mathbf{B}(\xi - \mathbf{x}_s) \text{ and } \mathbf{n}_{im} = \frac{1}{|l_{im}|}\mathbf{B}(\mathbf{x}_s - \eta), \tag{3.11}$$

respectively. Analogously, the outer normal vector $\mathbf{n}$ on the edge opposite node $\mathbf{x}_i$ can be expressed as

$$\mathbf{n} = \frac{1}{2}\mathbf{B}(\mathbf{x}_j - \mathbf{x}_m).$$

With (3.11) we get

$$\mathbf{n} = |l_{ij}|\mathbf{n}_{ij} + |l_{im}|\mathbf{n}_{im}. \tag{3.12}$$

In view of the property that the angles within the triangle are less or equal $90°$ there exist non-negative real numbers $\alpha, \beta \in \mathbb{R}_0^+$ such that

$$\mathbf{n} = \alpha(\mathbf{x}_m - \mathbf{x}_i) + \beta(\mathbf{x}_j - \mathbf{x}_i).$$

By equation (3.6) we get the inequality

$$\begin{aligned}
\Delta T_i|_{\mathcal{D}} &= \lambda_{\mathcal{D}} \nabla T_{\mathcal{D}}^T(t^n)\left(|l_{ij}|\mathbf{n}_{ij} + |l_{im}|\mathbf{n}_{im}\right) \\
&= \lambda_{\mathcal{D}} \nabla T_{\mathcal{D}}^T(t^n)\left(\alpha(\mathbf{x}_m - \mathbf{x}_i) + \beta(\mathbf{x}_j - \mathbf{x}_i)\right) \\
&= \underbrace{\lambda_{\mathcal{D}}}_{>0} \Big(\alpha \underbrace{\nabla T_{\mathcal{D}}^T(t^n)(\mathbf{x}_m - \mathbf{x}_i)}_{=T_m(t^n)-T_i(t^n)} + \beta \underbrace{\nabla T_{\mathcal{D}}^T(t^n)(\mathbf{x}_j - \mathbf{x}_i)}_{=T_j(t^n)-T_i(t^n)}\Big) \\
&\leq 0,
\end{aligned}$$

which concludes the proof. $\square$

Utilizing $|\mathcal{D}| \neq 0$ provides $\alpha + \beta > 0$. Taking into account $\sum_{i \in C(\mathcal{D})} \Delta T_i|_{\mathcal{D}} = 0$ we have

Lemma 3.2 *Consider an arbitrary triangle $\mathcal{D} \in \mathcal{D}^h$ and assume that the corresponding cell average $T_i(t^n)$, $i \in C(\mathcal{D})$ satisfies*

$$T_i(t^n) > \max_{j \in C(\mathcal{D}), j \neq i} T_j(t^n), \; \left(T_i(t^n) < \min_{j \in C(\mathcal{D}), j \neq i} T_j(t^n) \right).$$

Then, the local update of the cell average $T_i(t^n)$ associated with the triangle $\mathcal{D}$ satisfies

$$\Delta T_i|_{\mathcal{D}} < 0 \quad (\Delta T_i|_{\mathcal{D}} > 0).$$

Furthermore, there exists an index $j \in C(\mathcal{D})$ such that

$$\Delta T_j|_{\mathcal{D}} > 0 \;\; (\Delta T_j|_{\mathcal{D}} < 0).$$

The following Lemma substantiates the advantage of the specific adjusted evaluation of the boundary fluxes (3.9).

Lemma 3.3 *Let $i \in \mathcal{N}^{h,\partial D}$ and $j \in N(i) \cap \mathcal{N}^{h,\partial D}$, then the local update associated with the edge l_{ij}*

$$\Delta T_j|_{l_{ij}} = H_\nu(T_i(t^n), T_{i,\partial D}(\mathbf{x}_i), T_{i,\partial D}(\mathbf{x}_{ij}); \mathbf{n}_{ij}) \, |l_{ij}|$$

satisfies

$$\Delta T_j|_{l_{ij}} \leq 0 \quad \left(\Delta T_j|_{l_{ij}} < 0 \right)$$

if

$$T_i(t^n) \geq T_{i,\partial D} \quad (T_i(t^n) > T_{i,\partial D}).$$

Proof: Considering equation (3.8), the extended barycentre $\mathbf{c}_i$ of the box σ_i can be expressed as

$$\mathbf{c}_i = \mathbf{x}_i - \vartheta(\mathbf{n}_{ij} + \mathbf{n}_{im}), \; \vartheta \in \mathbb{R}^+. \tag{3.13}$$

From $T_{i,\partial D}(\mathbf{x}_i) = T_{i,\partial D}(\mathbf{x}_{ij})$ we obtain

$$\nabla T^T_{\mathcal{D}^c_{ij}}(t^n)(\mathbf{x}_{ij} - \mathbf{x}_i) = T_{i,\partial D}(\mathbf{x}_{ij}) - T_{i,\partial D}(\mathbf{x}_i) = 0$$

and the gradient can be written in terms of the outer unit normal vector $\mathbf{n}_{ij}$, namely

$$\nabla T_{\mathcal{D}^c_{ij}}(t^n) = \gamma \mathbf{n}_{ij}, \; \gamma \in \mathbb{R}. \tag{3.14}$$

Using $\mathbf{n}^T_{ij}\mathbf{n}_{im} > -1$ we obtain $\gamma \leq 0$ from the inequality

$$\begin{aligned} \gamma \left(1 + \mathbf{n}^T_{ij}\mathbf{n}_{im}\right) &= \gamma \left(\mathbf{n}^T_{ij}\mathbf{n}_{ij} + \mathbf{n}^T_{ij}\mathbf{n}_{im}\right) = \nabla T^T_{\mathcal{D}^c_{ij}}(t^n)(\mathbf{n}_{ij} + \mathbf{n}_{im}) \\ &\overset{(3.13)}{=} -\frac{1}{\vartheta}\nabla T^T_{\mathcal{D}^c_{ij}}(t^n)(\mathbf{c}_i - \mathbf{x}_i) = -\frac{1}{\vartheta}\left(T_i(t^n) - T_{i,\partial D}(\mathbf{x}_i)\right) \leq 0 \end{aligned} \tag{3.15}$$

Thus, one gets

$$\nabla T^T_{\mathcal{D}^{\mathbf{c}}_{ij}}(t^n)\mathbf{n}_{ij} = \gamma \leq 0$$

which directly proves $\Delta T_j|_{l_{ij}} \leq 0$. If $T_i(t^n) > T_{i,\partial D}$, we obtain $\gamma < 0$, and $\nabla T^T_{\mathcal{D}^{\mathbf{c}}_{ij}}(t^n)\mathbf{n}_{ij} < 0$ holds. □

We are now able to prove the first maximum principle which represents a discrete analogue of theorem 2.1.

Theorem 3.4 *Given a steady state $\Delta T = (\Delta T_1, \ldots, \Delta T_N)^T = \mathbf{0}$ of our finite volume method and an index $i \in \mathcal{N}^h$ such that*

$$T_i(t^n) = \max_{\ell \in \mathcal{N}^h, j \in \mathcal{N}^{h,\partial D}} \{T_\ell(t^n), T_{j,\partial D}\}, \tag{3.16}$$

we have

$$T_\ell(t^n) = T_i(t^n) = T_{j,\partial D} \text{ for all } \ell \in \mathcal{N}^h \text{ and } j \in \mathcal{N}^{h,\partial D}.$$

Proof: From Lemma 3.1 we conclude that $\Delta T_i|_{\mathcal{D}} = 0$ for all $\mathcal{D} \in V(i)$. Hence, from Lemma 3.2 we observe that for each $\mathcal{D} \in V(i)$ there exists at least one index $j \in C(\mathcal{D}) \setminus \{i\}$ such that $T_i(t^n) = T_j(t^n)$. Consequently, we have $\Delta T_j|_{\mathcal{D}} = 0$. By means of $\sum_{\ell \in C(\mathcal{D})} \Delta T_\ell|_{\mathcal{D}} = 0$ we obtain $\Delta T_\ell|_{\mathcal{D}} = 0$ for all $\ell \in C(\mathcal{D})$ which directly provides $T_i(t^n) = T_j(t^n)$ for all $j \in N(i)$. Successive repetition of the above described argumentation finally yields

$$T_i(t^n) = T_j(t^n) \;\; \forall j \in \mathcal{N}^h. \tag{3.17}$$

For $j \in \mathcal{N}^{h,\partial D}$ it follows from the assumption (3.16) in combination with equation (3.17) that $T_j(t^n) \geq T_{j,\partial D}$. Thus, Lemma 3.3 yields $\Delta T_j|_{l_{jm}} \leq 0$ for all $m \in N(j) \cap \mathcal{N}^{h,\partial D}$. With $\Delta T_j = 0$ we obtain $\Delta T_j|_{l_{jm}} = 0$. Inserting $\lambda_{\mathcal{D}^{\mathbf{c}}_{jm}} > 0$ into

$$\lambda_{\mathcal{D}^{\mathbf{c}}_{jm}} \nabla T^T_{\mathcal{D}^{\mathbf{c}}_{ij}}(t^n)\mathbf{n}_{jm} = \Delta T_j|_{l_{jm}} = 0$$

and using (3.14) provides a vanishing gradient $\nabla T_{\mathcal{D}^{\mathbf{c}}_{ij}}(t^n)$ and as a consequence we obtain $T_j(t^n) = T_{j,\partial D}$ which proves the statement. □

A close inspection of the proof above yields that the maximum as well as the minimum of the temperature distribution is always located on the boundary of the computational domain D. This fact proves the corollary below.

Corollary 3.5 *If the finite volume method yields $\Delta T = \mathbf{0}$, then there exist indices $j, m \in \mathcal{N}^{h,\partial D}$ such that*

$$T_{j,\partial D} = \max_{\ell \in \mathcal{N}^h, k \in \mathcal{N}^{h,\partial D}} \{T_\ell(t^n), T_{k,\partial D}\} \;\text{ and }\; T_{m,\partial D} = \min_{\ell \in \mathcal{N}^h, k \in \mathcal{N}^{h,\partial D}} \{T_\ell(t^n), T_{k,\partial D}\}.$$

4 Numerical Results

In this section we present some typical numerical results for the two-dimensional model (2.6).
To start with, we describe the triangulation of our computational domain D. Figure 1 displays the primary mesh for an infant of weight 1000 g. The triangulation is composed of about 37.000 triangles and 19.000 control volumes. As it is apparent from figure 2, a finer mesh was constructed for the skin, the fat, and the bone layer, respectively.
Next we present the physiological parameters used for our study. For a detailed description of these data we refer to Bußmann (2000) and references therein. The data used for the heat conductivity (λ) and the metabolic heat production (Q_M) are compiled in the following table.

Table 1: Heat conductivity in $[\frac{W}{mK}]$ and metabolic heat production in $[\frac{W}{m^2}]$.

	Heat conductivity	Heat production		
		Head	Body	Leg
Skin	0.35	0.0	0.0	0.0
Fat	0.21	0.0	0.0	0.0
Bone	0.40	0.0	0.0	0.0
Core	0.51	4500	1800	600

Furthermore, the data used for the blood-flow (BF) and the counter current factor (K_B) may be found in the next table.

Table 2: Blood-flow in $[\frac{1}{s}]$ and counter current factors.

	Blood-flow			Current factor		
	Head	Body	Leg	Head	Body	Leg
Skin	$1.25 \cdot 10^{-3}$	$1.25 \cdot 10^{-3}$	$1.25 \cdot 10^{-3}$	1.0	1.0	0.9
Fat	0.0	0.0	0.0	1.0	1.0	0.9
Bone	0.0	0.0	0.0	1.0	1.0	0.9
Core	0.0045	0.007	$1.25 \cdot 10^{-3}$	1.0	1.0	0.9

Finally, the specific heat and the density of the blood, respectively, were chosen as

$$c_B = 3840 \frac{J}{kgK} \text{ and } \rho_B = 1060 \frac{kg}{m^3}.$$

As outlined in Section 3, we employ an implicit time-marching procedure to reach the steady state solution. Therefore, we have to deal with an inner and an outer iteration scheme. The outer iteration was stopped once the discrete approximation

$$\begin{aligned} R_n &= \frac{1}{\Delta t}\left(\frac{1}{|D|}\sum_i (T_i(t^{n+1}) - T_i(t^n))^2|\sigma_i|\right)^{1/2} \\ &\approx \left(\frac{1}{|D|}\int_D \left|\frac{\partial T}{\partial t}\right| d\mathbf{x}\right)^{1/2} = \left\|\frac{\partial T}{\partial t}\right\|_{L_2(D)} \end{aligned} \quad (4.1)$$

of the $L_2(D)$ norm of the time derivative of the weak solution (cf. (3.2)) was brought below 10^{-8}.
Stability considerations easily prove that an explicit method has to satisfy $\Delta t = \mathcal{O}(h^2)$ in order to provide reliable numerical results even if the source terms are neglected. One can overcome this unfortunate feature by means of an implicit scheme ($\Theta_1 = 1$) which is unconditionally stable. Nevertheless, due to the truncation error of the order $\mathcal{O}\left(|\Delta T|^2\right)$ introduced by the incorporated linearization of the numerical flux function, it is usually advantageous to employ an appropriate time-stepping strategy also within the implicit approach. Hence, at the beginning of each time step we calculate the time step size for an explicit scheme and multiply this number by a factor which increases from 1 up to 500 during the computation to achieve fast convergence.
Each outer iteration step involves the solution of a sparse linear system. In accordance with the chosen triangulation, the associated matrix $\mathbf{A}$ is of the order 19.000. Each triangle has typically about 6-9 neighbors which amounts to 7-10 non-zeros entries per row in $\mathbf{A}$.
The performance of an implicit method decisively depends on the properties of the incorporated solver for the linear system of equations. For large and sparse matrices direct solvers are too expensive and thus iterative methods are required. Among the most well-known iterative solvers that are applicable to a (general) non-symmetric system are the Krylov subspace methods. Here, we tested the GMRES algorithm due to Saad and Schultz (1986) and the Bi-CGSTAB scheme developed by van der Vorst (1992), both preconditioned by an incomplete LU-factorization. For a detailed description and comparison of different Krylov subspace methods we refer to Saad (1996), Meister (1998, 1999).
The iteration was halted once the relative residual of the iterates was brought below 10^{-15}. It turns out that GMRES took roughly twice as much computing time than Bi-CGSTAB in all our test cases. Furthermore, it is interesting to note that, depending on the step size Δt, the schemes needed only about 4 to 35 iterations to achieve the desired accuracy. The results displayed in this section were obtained by using Bi-CGSTAB.
We present two test cases. They differ in the choice of the Dirichlet boundary conditions. Test case 1 was designed to reproduce the temperature distribution with respect to normal environmental conditions. In contrast, test case 2 models the attempt to lower the cerebral temperature by cooling the head.
To start the outer iteration, the initial temperature was chosen to be $310.15K = 37°C$ throughout the whole body.

Table 3: Dirichlet boundary conditions in $[K]$

	Head	Back	Leg	Belly
Test 1	309.15	310.15	307.65	309.15
Test 2	299.15	309.15	309.15	309.15

The next plot shows the convergence history of the outer implicit iteration for the two test cases.

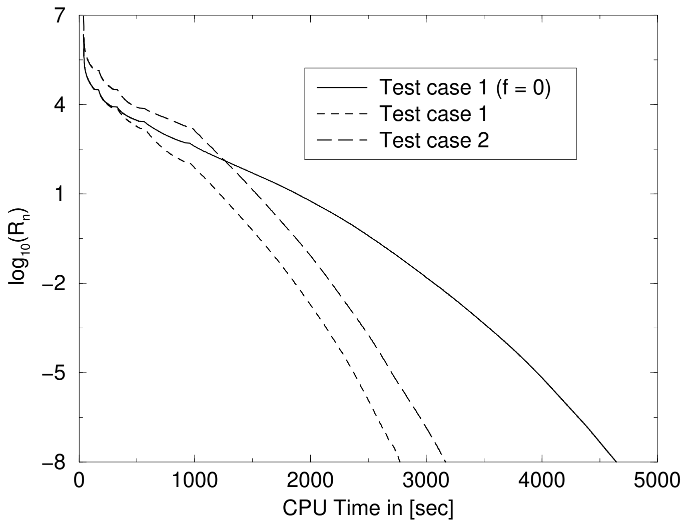

Figure 4: Computing time versus the residual $\log_{10}(R_n)$ for the two test cases.

It should come as no surprise that the implicit time-marching method converges rather smoothly to the steady state solution. Also it is worthwhile to note, that the overall computing time consumed by the corresponding explicit scheme to achieve the same accuracy was consistently about 50 times (!) higher.
Finally, let us visualize the obtained temperature distributions. To verify the discrete maximum principle, stated in Theorem 3.4, we first treat test case 1 without any heat production or blood-flow, i.e., $f(\mathbf{x}, t) = 0$. As it is apparent from the top image in figure 5, the maximal temperature occurs at the boundary of D, as predicted by our theory.
Regarding temperature distributions with heat production and blood-flow, depicted in the bottom part of figure 5, we observe that our model resembles nicely the expected temperature distribution with respect to normal environmental conditions. Most interestingly, figure 6 shows that a selective cooling of the head only affects the skin of the head, a result, which triggered a controversy discussion within the medical community. It is worth noticing that recently Bußmann (2000) obtained similar results in his computations. He considered a model with purely radial heat conduction but with more detailed governing equations.

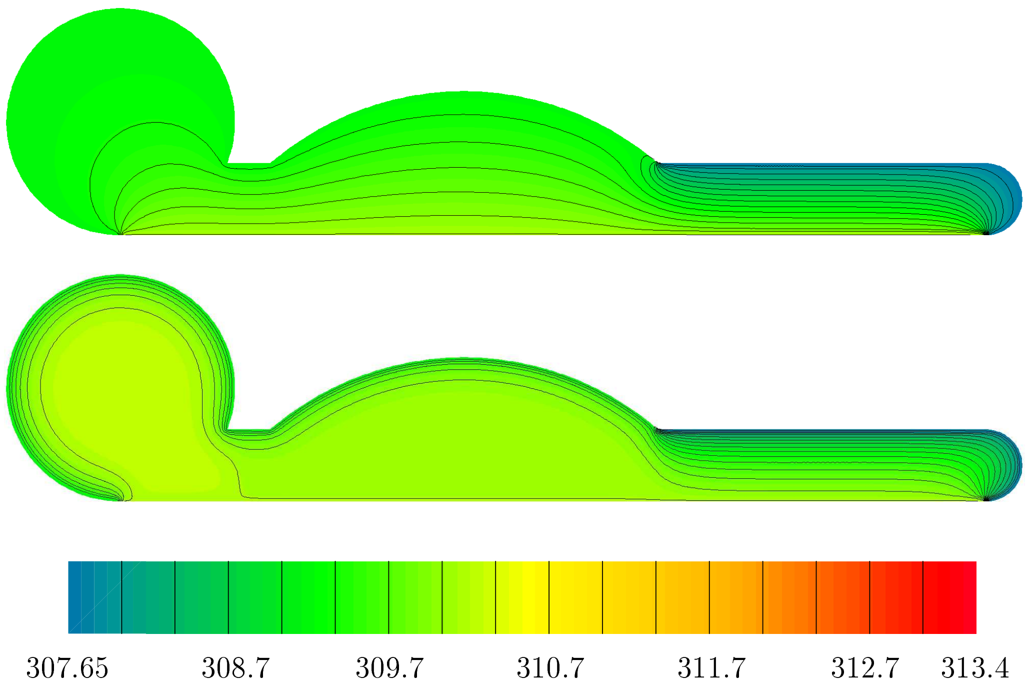

Figure 5: Temperature distribution for the test case 1 with $f = 0$ in the top figure.

5 Conclusions

An implicit finite volume method for the simulation of the thermoregulation of premature infants has been presented. The method has proven to be fast, stable, and reliable in the sense that the numerical steady state solution satisfies a discrete maximum principle also in the case of non-convex geometries. Several test cases based on real life data are considered to show the performance and applicability of the scheme. The validity of the results are recently confirmed by the work of Bußmann (2000). Hence, the proposed numerical algorithm represents an excellent basis for the computation of distinguish medical applications in the field of thermoregulation.

Acknowledgements

The authors would like to thank Dipl.-Ing. Otmar Bußmann, Institute of Biomedical Engineering, Medical University of Lübeck for providing the physiological data and for many helpful discussions. The authors gratefully acknowledge Dr. Jochim Koch, Drägerwerk AG, Dept. of Basic Development, Lübeck, for bringing the application to their attention and for his keen interest in the study. Furthermore, the authors wish to thank Dr. Oliver Friedrich, Institute of Applied Mathematics, University of Hamburg, for providing his excellent grid generator.
A. Meister would like to express his thanks to Dr. Michael Oevermann, Courant Institute of Mathematical Sciences, New York University, for proof reading parts of

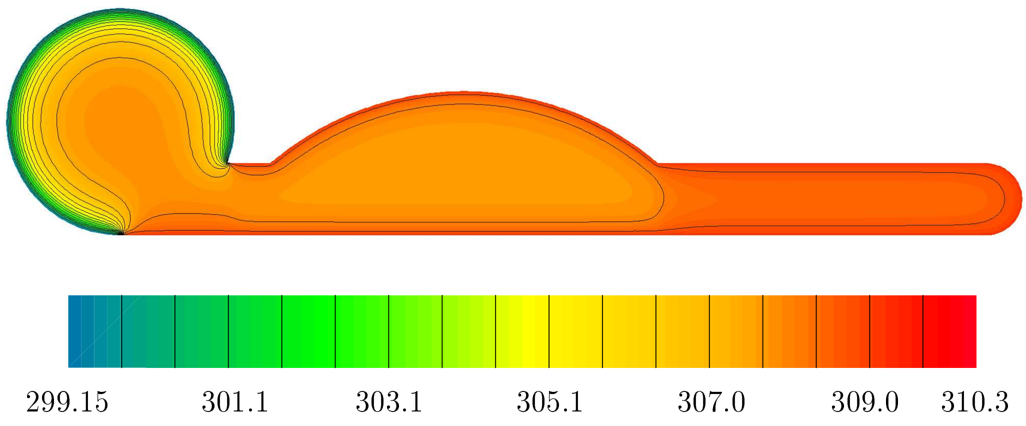

Figure 6: Temperature distribution for the test case 2.

the manuscript.

References

[1] O. Bussmann. *Modell der Thermoregulation des Früh- und Neugeborenen unter Einbeziehung der thermischen Reife.* Dissertation, Institute of Biomedical Engineering, Medical University of Lübeck, 2000.

[2] R. Busto, W. D. Dietrich, M. Y. Globus, M. D. Ginsberg. The importance of brain temperature in cerebral ischemic injury. *Stroke*, 20: 1134–1114, 1989.

[3] O. Friedrich. A new method for generating inner points of triangulations in two dimensions. *Comp. Meth. Appl Mech and Eng.*, 104: 77–86, 1993.

[4] P. D. Gluckman, C. E. Williams. When and why do brain cells die? *Dev. Med. Child Neurol.*, 34: 1010–1014, 1992.

[5] E. C. Mallard, C. E. Williams, B. M. Johnston, P. D. Gluckman. Neuronal damage in the developing brain following intrauterine asphyxia. *Reprod. Fertil. Dev.*, 7: 647–653, 1995.

[6] A. Meister. Comparison of Different Krylov Subspace Methods Embedded in an Implicit Finite Volume Scheme for the Computation of Viscous and Inviscid Flow Fields on Unstructured Grids. *J. Comput. Phys.*, 140: 311–345, 1998.

[7] A. Meister. *Numerik linearer Gleichungssysteme.* Vieweg, Wiesbaden, 1999.

[8] M. H. Protter, H. F. Weinberger. *Maximum principles in differential equations.* Prentice-Hall, Englewood Cliffs, New Jersey, 1967.

[9] Y. Saad. *Iterative Methods for Sparse Linear Systems.* PWS Publishing Company, Boston, 1996.

[10] Y. Saad, M. Schultz. GMRES: A generalized minimal residual algorithm for solving nonsymmetric linear systems. *SIAM J. Sci. Stat. Comput.*, 7: 856–869, 1985.

[11] Th. Sonar. On the Design of an Upwind Scheme for Compressible Flow on General Triangulations. *Numerical Algorithms*, 4: 135–149, 1993.

[12] Th. Sonar. On the Construction of Essentially Non-Oscillatory Finite Volume Approximations to Hyperbolic Conservation Laws on General Trinagulations: Polynomial Recovery, Accuracy, and Stencil Selection. *Comp. Meth. Appl. Mech. Eng.*, 140: 157–181, 1997.

[13] H. A. van der Vorst. BI-CGSTAB: A fast and smoothly converging variant of BI-CG for the solution of nonsymmetric linear systems. *SIAM J. Sci. Stat. Comput.*, 13: 631–644, 1992.

[14] J. Werner. Thermoregulatory models: recent research, current applications and future development. *Scand. J. Work. Environ. Health*, Vol.15: 34–46, 1989.

[15] J. Werner, P. Webb. A six-cylinder model of human thermoregulation for general use on personal computers. *Ann. Physiol. Anthrop.*, Vol.12 (3): 123–134, 1993.